MATERIALS SCIENCE

Bioinspired metagel with broadband tunable impedance matching

Erqian Dong[1]*, Zhongchang Song[1]*, Yu Zhang[1,2,3†], Shahrzad Ghaffari Mosanenzadeh[3], Qi He[3], Xuanhe Zhao[3], Nicholas X. Fang[3†]

To maximize energy transmission from a source through a media, the concept of impedance matching has been established in electrical, acoustic, and optical engineering. However, existing design of acoustic impedance matching, which extends exactly by a quarter wavelength, sets a fundamental limit of narrowband transmission. Here, we report a previously unknown class of bioinspired metagel impedance transformers to overcome this limit. The transformer embeds a two-dimensional metamaterial matrix of steel cylinders into hydrogel. Using experimental data of the biosonar from the Indo-Pacific humpback dolphin, we demonstrate through theoretical analysis that broadband transmission is achieved when the bioinspired acoustic impedance function is introduced. Furthermore, we experimentally show that the metagel device offers efficient implementation in broadband underwater ultrasound detection with the benefit of being soft and tunable. The bioinspired two-dimensional metagel breaks the length-wavelength dependence, which paves a previously unexplored way for designing next-generation broadband impedance matching devices in diverse wave engineering.

INTRODUCTION

Acoustic materials have made substantial progress in recent years. Metamaterials provide a powerful tool to design physical properties through programmable design of microstructure (*1*–*5*). This may result in a variety of novel effects, such as negative refraction, invisibility cloaking, and other extraordinary transmissions. Introducing soft materials to acoustics makes it possible to avoid the rigid feature of solid structures (*6*–*10*), giving more freedom during design. Because of its soft, wet, and biocompatible nature, hydrogel has been applied in tissue engineering, soft robotics, and soft electronics. Hydrogel has nearly perfect acoustic impedance matching with water because more than 90% of its constituent is water. This property makes hydrogel a good background matrix material for composite designs in underwater applications (*8*). A recent study has proposed a design of metagel by fabricating one-dimensional patterned channels in a hydrogel to tune the acoustic transmission in air-water-solid impedance ranges (*9*). However, as far as we know, there are no reports on two-dimensional hydrogel metamaterials capable of establishing broadband acoustic transmission between two mismatching media.

Impedance matching maximizes energy transmission between two mismatching media, which has received considerable attention in the science and technology community. In the early 20th century, Bell Laboratories discovered the importance of impedance matching to make transcontinental telephone communication practical (*11*). Ever since, impedance matching has been applied in electrical, mechanical, acoustic, optical, microwave engineering, etc. Quarter-wave impedance transformer (QIT) with a length of $L = \lambda/4$ (L is the length and λ is the wavelength in the matching layer) has been widely applied to maximize energy transmission (*12*–*17*). The matching layers of acoustic transducers have been commonly used in underwater sonar, ultrasonic transducer, and medical ultrasonic sensor (*18*, *19*, *20*). The acoustic impedance (Z_0) of a piezoelectric transducer is about 22 times higher than that of water (Z_1), resulting in an energy transmission as low as 17%. It is necessary to apply acoustic impedance matching layer (Z_T) to couple Z_0 with Z_1 to improve energy transmission. Total transmission power of QIT ($T = 1$) requires $Z_T^2 = Z_0 \times Z_1$ and the following length-wavelength dependency (see Materials and Methods) (*21*)

$$\lambda = KL \tag{1}$$

where K is a coefficient. QIT satisfies $K = 4/(2n - 1)$, ($n = 1,2, \cdots$), and thus, this length-wavelength relationship sets the fundamental transmission limit, which results in most existing transformers as narrowband matching devices. To improve matching performance, multiple layers and acoustic metamaterials have been designed (*18*, *19*, *20*). However, to achieve a tunable and broadband transmission is still a great challenge to these transformers due to their rigid feature.

Nature may have found a way to overcome the narrowband transmission as is suggested to be the case in dolphin's biosonar systems (*22*, *23*). Dolphins have evolved a sophisticated biosonar system to adapt to the underwater environment (*24*–*27*). Dolphins generate broadband signals by the monkey lips/dorsal bursae complex in their nasal system to prey and detect underwater objects (*25*). Their foreheads, as a soft impedance matching system, can transmit broadband signals into water (*26*). The acoustic transmission of dolphin biosonar is manipulated by its acoustic impedance distribution in the forehead. Fatty tissues, muscles, and connective tissues are stacked in a typical order to create a certain acoustic impedance distribution. Fatty tissues own the lowest acoustic impedance and constitute the innermost layer in the forehead. They are wrapped peripherally by muscle tissues, which have a higher acoustic impedance. Connective tissues have the highest acoustic impedance and resemble a complex horn-like structure in the posterior forehead. These tissues produce an acoustic impedance

[1]Key Laboratory of Underwater Acoustic Communication and Marine Information Technology of the Ministry of Education, College of Ocean and Earth Sciences, Xiamen University, Xiamen 361005, China. [2]State Key Laboratory of Marine Environmental Science, Xiamen University, Xiamen 361005, China. [3]Department of Mechanical Engineering, Massachusetts Institute of Technology, Cambridge, MA 02139, USA.
*These authors contributed equally to this work.
†Corresponding author. Email: yuzhang@xmu.edu.cn (Y.Z.); nicfang@mit.edu (N.X.F.)

variance to control energy transmission (*24*). In particular, dolphins can adjust their forehead through compressing facial musculature to produce tissue deformations (*27*). Thus, acoustic directivity can be manipulated by compressing melon and surrounding tissue as a tunable structure (*28*).

Here, we report that the narrowband limit can be overcome by a bioinspired metagel impedance transformer (BMIT). Inspired by the impedance distribution of a dolphin, we obtain the gradient acoustic impedance function of BMIT. Hydrogel is fabricated and embedded into a matrix of steel cylinders to design a metamaterial. Hydrogel plays a significant role in the tunable device. The broadband matching mechanism of the two-dimensional metagel is theoretically and experimentally demonstrated. This novel bioinspired device integrates the features of metamaterial and hydrogel.

RESULTS AND DISCUSSION

Gradient acoustic impedance distribution in the head of an Indo-Pacific humpback dolphin was reconstructed using computed tomography scanning and tissue experiments (Fig. 1A and fig. S1). The core region, which owns a low acoustic impedance, acts as an acoustic channel to guide energy flux along its direction. This channel was numerically confirmed in acoustic fields using full-wave simulations (see Materials and Methods). The impulse signal transmitted by the channel clearly presents a broadband spectrum (fig. S3). The impedance function was then obtained from the dolphin's impedance data as $\gamma(x) = \gamma_0 + \varepsilon e^{ax}$, where x represents the acoustic propagation direction and γ_0, ε, and a are coefficients determined as $\gamma_0 = 0.44$, $\varepsilon = 0.47$, and $a = -1.83/L$ to fit the real impedance data [coefficient of determination (R^2) = 0.91] in Fig. 1B.

Inspired by the biosonar property of the dolphin, we obtained the acoustic impedance function of BMIT to couple water at $x = 0$ with the source [such as piezoelectric (PZT)] at $x = -L$ as

$$\gamma(x) = \gamma_0 + \varepsilon \left[\frac{\varepsilon}{Q - \gamma_0}\right]^{x/L} \quad (2)$$

where $Q = Z_0/Z_1$ is the ratio of transducer impedance over water impedance. To mimic the deformable forehead of the dolphin, a two-dimensional metagel structure has been designed (the top curve in Fig. 1C) to achieve effective acoustic impedance of Eq. 2. The matrix of steel cylinders is embedded in a hydrogel with lattice constant a = 0.02 m. Diameter profile of the cylinders is shown in the bottom part of Fig. 1C. According to the effective medium theory (*3*, *29*, *30*), programming the filling ratio or the diameter of the steel cylinders provides an efficient way to change effective density, sound speed, and acoustic impedance of metagel (*9*). In addition, the impedance profile of BMIT is tunable by compressing the hydrogel.

First, we numerically demonstrated how the BMIT achieved broadband impedance matching. In Fig. 1 (D and E), the simulated acoustic fields of BMIT and QIT are compared. When f_0 = 60 kHz, BMIT effectively transmits the acoustic wave, while QIT shows a low energy transmission. When f_0 = 120 kHz, BMIT and QIT both have high transmission. In particular, BMIT provides a broadband frequency response, differing from the narrowband transmission of QIT (Fig. 1F). We calculated the 3-dB bandwidth, which describes

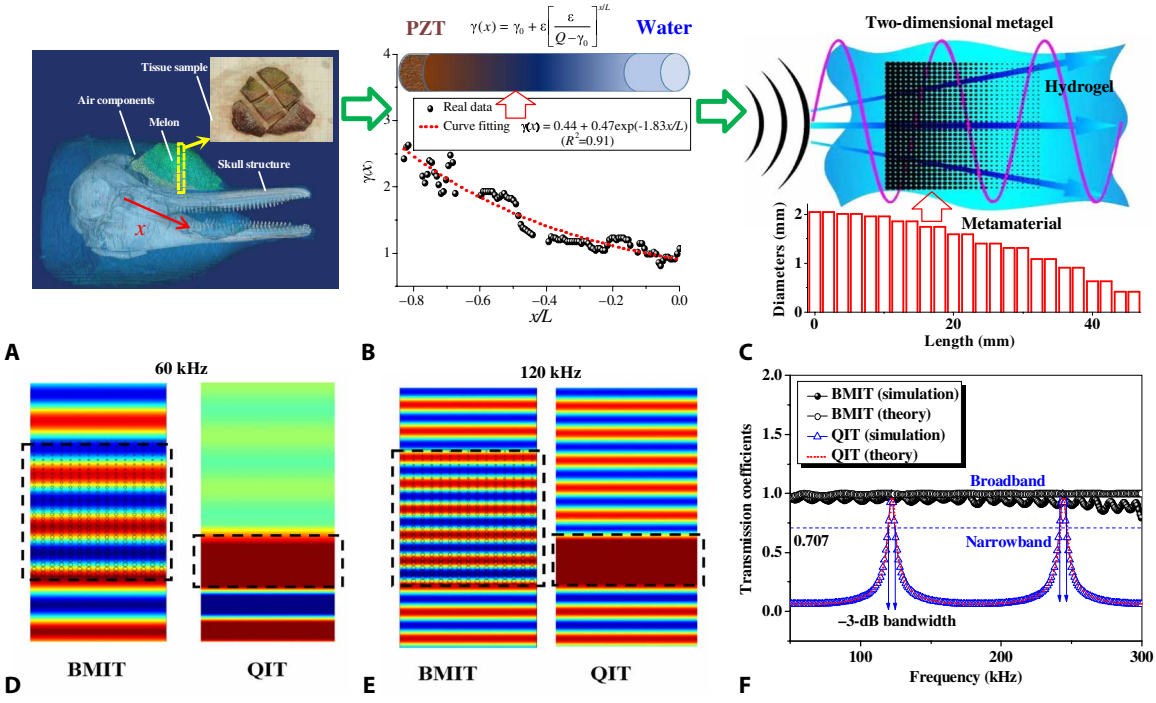

Fig. 1. A design of BMIT based on dolphin's structure. (**A**) Three-dimensional acoustic impedance distribution of the dolphin's head and a sectioned tissue sample (photo credit: Zhongchang Song). (**B**) Acoustic impedance profile of the channel and its fitting curve for obtaining the impedance function of BMIT as $\gamma(x) = \gamma_0 + \varepsilon \left[\frac{\varepsilon}{Q-\gamma_0}\right]^{x/L}$ to couple water at $x = 0$ with PZT at $x = -L$. (**C**) Schematic illustration of the two-dimensional metagel structure and the corresponding diameter profile of steel cylinders. (**D**) Acoustic field comparison between the numerical simulations of BMIT and QIT at the frequency of $f_0 = 60$ kHz. (**E**) Acoustic field comparison between BMIT and QIT at the frequency of $f_0 = 120$ kHz. (**F**) Frequency response comparison between the numerical simulations and theoretical solutions of BMIT and QIT.

the bandwidth between two frequency points, in which spectrum amplitude reduced to half, to further compare the frequency responses of transmission between these two designs. Within the frequency range from 50 to 300 kHz, the 3-dB bandwidth of BMIT and QIT were calculated as 250 and 5 kHz, respectively. Clearly, BMIT had a much larger 3-dB bandwidth than QIT. The fluctuation of the simulated BMIT (Fig. 1F) may be associated with the multiple scattering effect of the metal cylinder matrix. According to the effective medium theory, the metagel requires a long-wavelength approximation. In our metagel design, the sound speed in metal cylinder matrix is 6400 m/s. When the lattice constant of the cylinders was a = 0.02 m, which was less than the wavelength, it led to an upper cutoff frequency of about 300 kHz as shown in Fig. 1F. The upper cutoff frequency could be increased by reducing a. For example, when a = 0.01 m, the high cutoff frequency could be estimated to be 640 kHz. Numerical simulations and theoretical solutions show a good qualitative agreement. Thus, the two-dimensional metagel fabricated by bioinspired impedance function has the advantage of broadband matching.

To reveal the impedance matching mechanism of BMIT, we applied the nonuniform transmission line equation (see Materials and Methods)

$$\frac{\partial R(x)}{\partial x} - 2ikR(x) + \frac{\varepsilon\, ae^{ax}}{2(\gamma_0 + \varepsilon\, ae^{ax})}[1 - R^2(x)] = 0 \qquad (3)$$

where $i^2 = -1$, k is the wave number in free space and R is the reflection coefficient. QIT represents a special case of Eq. 3 at $\varepsilon = 0$ and $\gamma_0 = \sqrt{Q}$. It produces a total transmission if L is odd multiples of $\lambda/4$, indicating narrowband property (Fig. 2A). The lowest transmission frequency $\omega_c = \pi c/2L$ of QIT corresponds to $\lambda = 4L$ (*12*), while BMIT may have a higher cutoff frequency. BMIT describes the nonuniform medium with spatially varying impedance to accomplish desired functionality. For weakly nonuniform impedance transformers ($\varepsilon << 1$), the transmission still obeys the length-wavelength restriction according to the small impedance perturbation theory (see Materials and Methods). For significantly nonuniform materials, recent studies have found that invisibility cloaking and acoustic mirage could be obtained by designing anisotropic inertia as well as elasticity using transformation acoustics (*2*). In the present study, we obtained broadband transmission by designing gradient impedance using dolphin's function. Exponential horn with expanded profile has been widely used in the air to improve the energy transmission (*18*, *19*). Horns may achieve acoustic transmission through a curved solid boundary. However, we design the metagel as a two-dimensional flat structure. The transmission of BMIT may not be analytically solved by the Riccati equation as shown in Eq. 3, while the transmission of the exponential horn can be analytically solved. According to the transformation acoustics, the impedance function can be transformed by acoustic characteristic impedance with geometric deformation. Although its impedance function may not be exactly exponential, and the acoustic-solid coupling should be considered in this underwater device, the metagel may represent a compressed-space version of the horn structure. From the small reflection theory, $L/\lambda >> 1$ leads to the approximate solution to be close to the BMIT response (see Materials and Methods). Clearly, T approaches to 1 if $L/\lambda >> 1$. In comparison with uniform material, the impedance gradient material significantly suppresses the reflection. Length and wavelength of BMIT are independent, that is, $\lambda \neq KL$. Analogous to the independent relationship between response time and bandwidth in resonant systems overcoming the time-bandwidth limit (*31*), BMIT breaks the length-wavelength dependency in Eq. 1 (Fig. 2A).

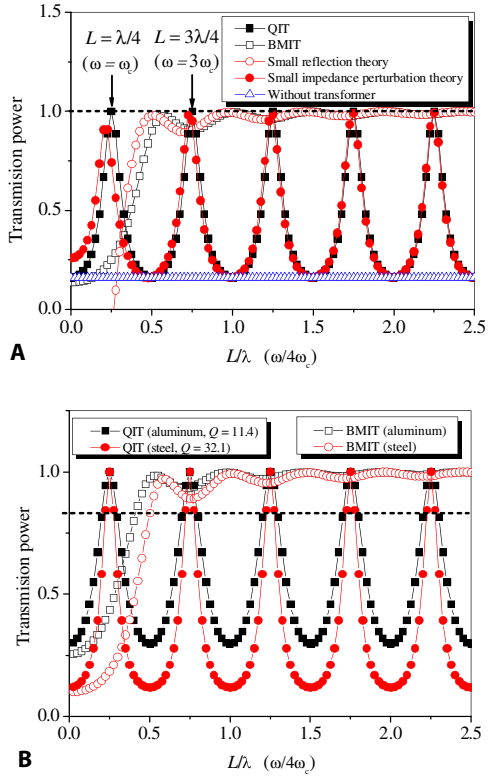

Fig. 2. BMIT capable of overcoming the narrowband limit for impedance matching. (**A**) Dependencies of the transmission powers of the mismatched system, QIT, and BMIT on L/λ, where L/λ corresponds to $\omega/4\omega_c$, Q = 22.8 is used for the PZT transducer, and the approximate solutions of BMIT from the small reflection and small impedance perturbation theories are also given. (**B**) Dependencies of the transmission powers of QIT and BMIT on L/λ, where Q = 11.4 and 32.1 correspond to aluminum and steel, respectively.

In particular, the broadband performance of BMIT is not affected by changing the gradient of $\gamma(x)$ (Fig. 2B). We increase Q from 11.4 (aluminum) to 32.1 (steel). QITs fabricated by different materials show resonant and narrowband transmissions; however, BMITs demonstrate broadband performances. Other materials such as copper, gold, and quartz were also examined (fig. S4), suggesting the general application of BMIT.

To further verify the broadband impedance matching applications of BMIT, we experimentally fabricated a two-dimensional hexagonal array of steel cylinders embedded in an agarose hydrogel (Fig. 3A and fig. S7A). Acoustic impedance of the agarose hydrogel is close to that of dolphin's tissue (fig. S2). The diameter of the cylinders in BMIT (D) progressively increases to approach the impedance function in Fig. 1B. A linear correlation between the composite impedance and the bioinspired function in Eq. 2 was found. Cylinder diameters are smaller than incident wavelength, and thus, the hydrogel-steel composite structure is a two-dimensional metamaterial (*32*).

Acoustic impedance of the designed BMIT is tunable through either changing the filling ratio of the metallic cylinders or compressing the hydrogel (Eq. 18). The two-dimensional metagel was uniformly compressed along the x-axis direction as $L = L_0(1 + \Delta)$,

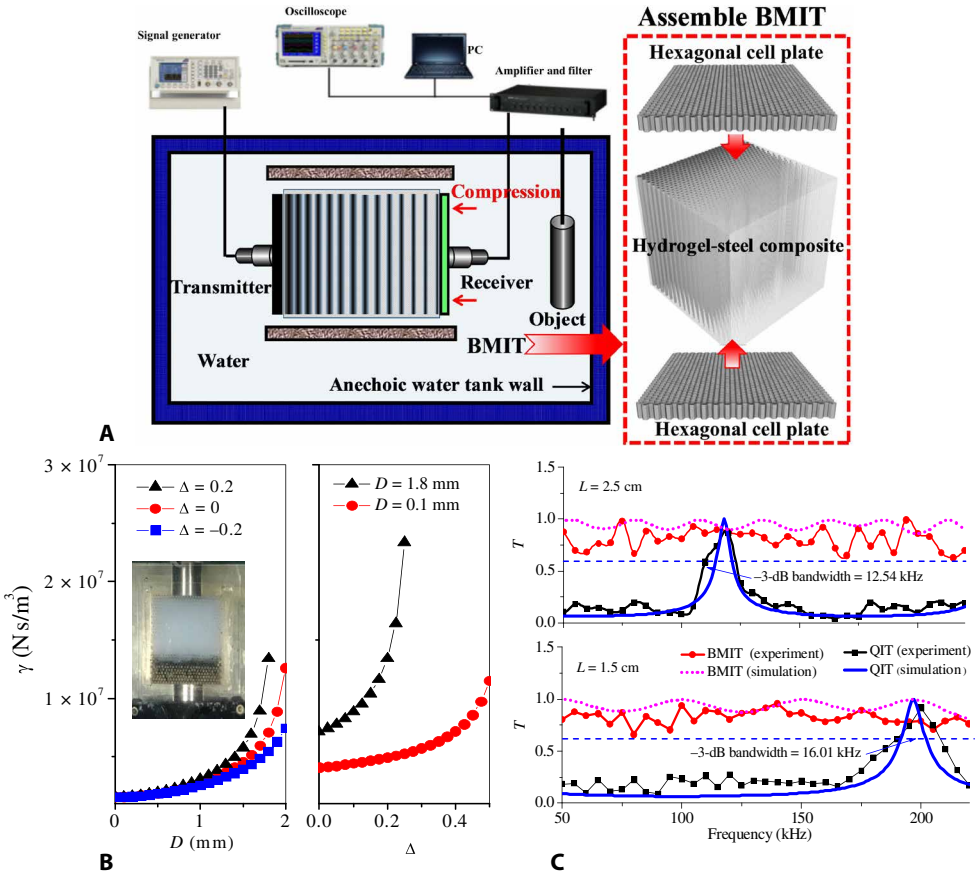

Fig. 3. Experimental measurement of BMIT for broadband transmission. (**A**) Systematic diagram of the experimental setup and the procedure to assemble a hydrogel with a two-dimensional hexagonal array of steel cylinders. (**B**) Effects of cylinder diameter and compression ratio on acoustic impedance (photo credit: Erqian Dong). (**C**) Frequency response comparisons between the experimental measurements and numerical simulations of QIT and BMIT, where the top and bottom curves correspond to $L = 2.5$ and 1.5 cm, respectively.

where Δ is the compression ratio of the current length L to the original length L_0. Acoustic impedance of the metamaterial increases with D and Δ (Fig. 3B and fig. S6). Hydrogel as a soft material offers the advantage of flexibly tuning acoustic impedance of BMIT.

We then performed underwater ultrasound transmission experiments in a water tank with a dimension of 1.2 m by 1.2 m by 1 m (Fig. 3C and fig. S7). QIT and BMIT transmitted tone-burst acoustic signals. Both frequency and length dependencies were observed in the experimental and numerical results of QIT. For the measured QIT, the 3-dB bandwidths were about 12.54 and 16.01 kHz for $L = 2.5$ and 1.5 cm, respectively. For the simulated QIT, the 3-dB bandwidths are about 5.0 and 8.3 kHz for $L = 2.5$ and 1.5 cm, respectively. The damping within the real material might have caused the bandwidth difference between experimental and numerical results for QIT. Another reason would be the difference of frequency resolution between experiments and simulations. A step of 5 kHz was used in experiments, while the frequency resolution was 1 kHz in simulations. Despite these influences, numerical and experimental results were qualitatively consistent. However, the broadband transmission was observed in BMIT and was not influenced when compressing the transformer. Within the measured frequency range of 50 to 230 kHz, the 3-dB bandwidths of the simulated and measured BMITs were about 180 kHz. BMIT maximizes the transmission performance of the acoustic transducer. Experimental results show good agreements with the numerical simulations. In other words, BMIT has the broadband advantage even when the structure length is changed.

We lastly show an underwater ultrasound detection application by using BMIT and QIT to couple an echosounder transducer with water (Fig. 4). The time-distance acoustic backscatter intensity profiles were given to locate an iron cylinder object at the distance of 35 cm and a steel wall at the distance of 80 cm from the transducer. For QIT, the steel wall was not detected by the echosounder under the condition of an immobile object (II), while it was both visible in the case without the object (I) and in the case with a swaying object (III). The object was difficult to be detected in both (II) and (III). The echo intensity of $L = 1.5$ cm in Fig. 4B was much less than that of $L = 2.5$ cm in Fig. 4A. However, for BMIT, higher intensity signals were transmitted, and then longer detection distances were obtained. The echosounder can more clearly locate the steel wall in (I), (II), and (III). The immobile object in (II) was detected. The swaying behavior of the object in (III) was tracked. The difference of tracking performance for BMIT with $L = 1.5$ and 2.5 cm might be associated with the incident acoustic intensity change as shown in Fig. 4 (A and B). However, under the same acoustic incident intensity, BMIT had a better performance than QIT for both $L = 1.5$ and 2.5 cm. The steel wall and the targets were both readily detected by the echosounder with BMIT. The broadband impedance matching

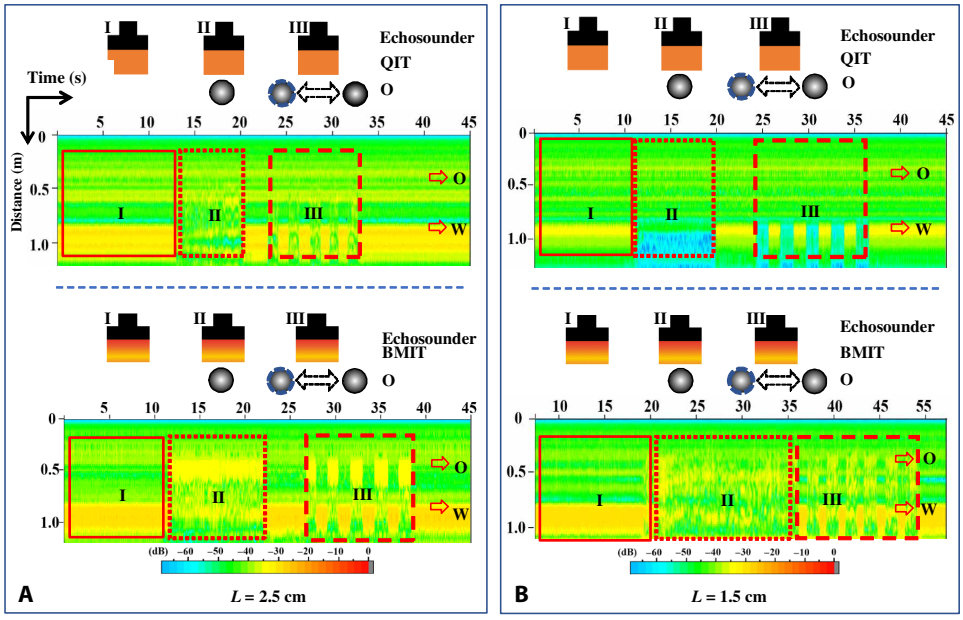

Fig. 4. Broadband impedance matching application of BMIT in underwater ultrasound detection. (**A**) and (**B**) correspond to *L* = 2.5 and 1.5 cm, respectively, and "W" and "O" represent steel wall and iron object, respectively. QIT and BMIT are coupled with the echosounder to range the following cases: (I) without object, (II) with an immobile object, and (III) with a swaying object.

of BMIT thus advocates for applications in underwater acoustic sensing.

Conclusions

We demonstrate that BMIT overcomes the narrowband limit by breaking the length-wavelength dependency. This impedance matching design is inspired from the dolphin's biosonar. The dolphin's biosonar is a complex three-dimensional impedance transformer (*23*, *28*). Bioinspired two-dimensional metagel allowing for broadband impedance matching can enhance energy transmission. Previous gradient metamaterials have applied solid structures to form directivity patterns (*29*, *30*) and to slow down waves (*33*, *34*), and the filling ratio may not be changed by compressing the structures (*1*, *3*, *5*, *14*, *15*, *32*). In this study, we focus on impedance matching of bioinspired metagel to maximize wave transmission instead of directivity. Plane wave has been applied in model simulations and experiments. We have not investigated how metagel could control directivity and have not explored the possibility of anisotropic metagel to simultaneously achieve the impedance matching and directivity control. Further study is needed to study this interesting topic. In addition, the bioinspired device offers attractive features, such as hydrogel, metamaterial, and tunability. Hydrogel holds the position and shape of the composites (*8*, *9*, *35*, *36*). The acoustic impedance of the metagel is adjustable by assigning different compression levels while still maintaining a broadband acoustic transmission. This offers an advantage that the compressed metagel can match different background impedance for broadband transmission, which is a challenge to solid transformers (*1*–*6*). Last, in many ultrasound or radar applications, broadband transmissions are needed to improve temporal and spatial resolutions. QIT and multiple matching layers are often incompetent in application because of their limited bandwidths. BMIT provides a new framework to design a broadband impedance transformer for high-resolution sonar or radar by decoupling length and wavelength. As an analogy between electromagnetic and acoustic waves (*37*), this bioinspired metagel technique for broadband and tunable impedance matching can have great implications in diverse areas including acoustics, mechanics, electronics, and electromagnetism.

MATERIALS AND METHODS

Measurement of acoustic impedance distribution within the head of an Indo-Pacific humpback dolphin using computed tomography scanning and tissue experiments

A dead female Indo-Pacific humpback dolphin with a body length of 2.7 m and a weight of 280 kg was found stranded in Quanzhou waters on 14 March 2015 (*24*). Computed tomography scanning of the dolphin's head with a slice width of 0.625 mm was carried out at the Radiology Department of Affiliated Zhongshan Hospital of Xiamen University. All images were collected with a power setting of 120 kV × 600 mA and with a matrix size of 512 × 512. Hounsfield unit (HU) in the computed tomography images was obtained by comparing the linear attenuation coefficient of a voxel with that of water. The tissues denser than water would have higher HU values. The high-resolution computed tomography imaging allowed us to extract the fine anatomical structure of the dolphin, and then the axial cross section, coronal cross section, and sagittal cross section were presented (fig. S1).

Furthermore, the acoustic impedance being the product of tissue density and sound speed was obtained from the tissue experiments. The forehead soft tissues were sectioned into 10 transverse slices, which were further cut into 42 small pieces. The sample weights *m* were measured by an electronic balance with an accuracy of 0.001 g. The volumes *V* were measured by a measurement cylinder with an accuracy of 1 ml. The density $\rho = m/V$ of each tissue was determined. In addition, the sound speeds of these tissue samples were measured

by using an ultrasound velocimeter with a pulse frequency of 3.5 MHz at room temperature. The tissue thickness d was measured with a vernier caliper. The acoustic travel time $t = t_2 - t_1$ within each tissue was measured with an oscilloscope, as shown in fig. S2, where t_1 represents the first reflected pulse at the upper surface of the tissue and t_2 represents the second reflected pulse at the lower tissue surface. On the basis of the measured m, V, d, and t, the acoustic impedance of the tissue sample was computed as

$$\gamma = 2 \times \frac{md}{Vt} \tag{4}$$

The acoustic impedance of each sample was measured five times to obtain the average value. HU and the acoustic impedance of one tissue sample were measured as 91.5 and 1.654×10^6 Pa·s/m, respectively. Air has low acoustic impedance of 4.15×10^2 Pa·s/m, while the skull has high acoustic impedance of 6.241×10^6 Pa·s/m. Recent study has found that the HU values of soft tissues were linearly related to the acoustic impedance (*24*); therefore, combing computed tomography imaging with tissue experiment, the gradient acoustic impedance distribution within the dolphin's head was obtained (Fig. 1A).

Acoustic field simulation of the dolphin model and BMIT

Finite element simulation was applied to perform full-wave simulation of the acoustic transmission processes within the dolphin's head. In the fluid media (such as air, water, melon, and other soft tissues), only longitudinal waves will propagate, which can be described by the wave equation

$$\frac{1}{\rho_0 c_s^2}\frac{\partial^2 p}{\partial t^2} + \nabla \cdot \left(-\frac{1}{\rho} \nabla p \right) = 0 \tag{5}$$

where p is the sound pressure, ρ_0 is the density, and c_s is the sound speed. A variable density ρ is included, since the forehead complex is inhomogeneous. In the skull structures, both shear and compressional waves should be considered as

$$\rho \frac{\partial^2 \mathbf{v}}{\partial t^2} = (\lambda + \mu) \nabla (\nabla \bullet \mathbf{v}) + \mu \nabla^2 \mathbf{v} \tag{6}$$

where $\mathbf{v}$ is the velocity vector and λ and μ are the two Lamé constants, characterizing compression and shear moduli, respectively. The acoustic fields in fig. S3A were numerically derived by solving these wave equations with proper boundary conditions using COMSOL Multiphysics Modeling software (Stockholm, Sweden) (*28*, *29*). The sound speed and density of the tissues were obtained by computed tomography imaging and tissue experiments. The boundary conditions require that the sound pressure and normal velocity at the boundary of the fluid media are continuous, while normal velocity and mechanical stress at the skull-tissue boundary are continuous.

Furthermore, to numerically investigate the broadband performance, a short-duration pulse was used as

$$p_s = \begin{cases} e^{\alpha_1 t} \sin(2\pi f_0 t) & 0 \le t \le t_0 \\ e^{[-\alpha_2 t + 2\alpha_2 t_0)]} \sin(2\pi f_0 t) & t_0 \le t \le 3t_0 \\ 0 & 3t_0 \le t \end{cases} \tag{7}$$

where α_1 and α_2 are the attenuation factor, f_0 is the peak frequency, and $t_0 = 1/f_0$ is the point at which the signal reaches the highest value. For the short-duration pulse in fig. S3B, the transmitted signal by the acoustic channel shows the broadband spectrum in Fig. 1C, where $\alpha_1 = 4 \times 10^4$ and $\alpha_2 = 2 \times 10^5$. The central frequency f_0 was set as 100 kHz according to our field measurement of the Indo-Pacific humpback dolphin in Xiamen Bay. Using the finite element simulation, full-wave simulations of BMIT for the impulse signal were performed for comparison with QIT, where the gradient impedance function was realized by setting the density function $\rho(x) = \left[a + d\, e^{-\ln\left(\frac{b-a}{d}\right)x/L}\right]/c$ kg/m^3, and the following parameters were used as sound speed $c = 2000$ m/s, $a = 0.01Z_1$, $d = 0.99Z_1$, $b = Z_0$, $Z_0 = 33.5 \times 10^6$ Pa·s/m, and $Z_1 = 1.48 \times 10^6$ Pa·s/m, respectively. Differing from the narrowband of QIT, the more broadband transmitted signal of BMIT was then obtained using this method (Fig. 1D and fig. S3D).

Nonuniform transmission line theory of BMIT

For one-dimensional transverse electromagnetic and acoustic waves, the spatial distribution of the reflection coefficient within an impedance gradient medium could be described in a unified way, by a nonlinear differential equation (*13*, *18*)

$$\frac{\partial R(x)}{\partial x} - 2ikR(x) + \frac{1}{2}\frac{\partial [\ln \gamma(x)]}{\partial x}[1 - R^2(x)] = 0 \tag{8}$$

where $i^2 = -1$, R is the reflection coefficient, and $\gamma(x)$ is the gradient acoustic characteristic impedance. To couple the transducer with water, the impedance of both sides of BMIT satisfy $\gamma(-L) = Q$ and $\gamma(0) = 1$ and thus have $T = 1 - |R(-L)|^2$.

For the uniform medium with impedance γ_0, Eq. 8 was reduced to

$$\frac{\partial R(x)}{\partial x} - 2ikR(x) = 0 \tag{9}$$

leading to the solution $R_0 e^{2ikx}$, where $R_0 = \frac{\gamma_0 - 1}{\gamma_0 + 1}$ was determined by the boundary impedance γ_0 at $x = 0$. QIT had $\gamma_0 = \sqrt{Q}$, and then we had the following relationship for $T = 1$

$$\lambda = \frac{4L}{2n-1}, \quad (n = 1, 2, \cdots) \tag{10}$$

We thus had Eq. 1 to describe the length-wavelength relationship.

However, for the impedance gradient medium of BMIT, Eq. 8 is a Riccati equation whose analytical solution is difficult to obtain except for quite few transformers, such as an exponential transformer (*18*). Substituting $\gamma(x) = \gamma_0 + \varepsilon e^{ax}$ into Eq. 8, we then obtained Eq. 3. Numerical solutions in Fig. 3 were obtained by applying a fourth-order Runge-Kutta method to numerically integrate Eq. 3, where the boundary condition was $R(0) = R_0$ and the integration step was $L/10{,}000$.

In addition, we also used the approximate theories of small reflections (*18*) as well as small impedance perturbations (*19*) to derive the approximate solutions. For small reflection approximation $R << 1$, Eq. 3 was reduced to

$$\frac{\partial R(x)}{\partial x} - 2ikR(x) + \frac{\varepsilon a e^{ax}}{2(\gamma_0 + \varepsilon e^{ax})} = 0 \tag{11}$$

and then $R(x)$ was solved as

$$R(x) = \frac{\varepsilon a}{2} e^{2ikx} \int_0^{-L} \frac{e^{(a-2ik)x}}{(\gamma_0 + \varepsilon e^{ax})} dx + C \quad (12)$$

where C is the constant determined by the reflection coefficient R_0 at $x = 0$. For the matched impedance at $x = 0$, $R_0 = 0$ led to $C = 0$. $L/\lambda >> 1$ led to $T \to 1$. It could be more clearly seen when $\gamma_0 = 0$. In this case, Eq. 12 was solved as $R(-L) = \frac{a}{4ik}[e^{-2ikL} - 1]$. When $\gamma_0 \neq 0$, Eq. 12 was solved as $R(-L) = e^{-2ikL} \frac{\varepsilon a e^{a\xi}}{2(\gamma_0 + \varepsilon e^{a\xi})} \int_0^{-L} e^{-2ikx} dx$, according to the integral mean value theorem, where $\varepsilon a e^{a\xi}/(\gamma_0 + \varepsilon e^{a\xi})$ is a continuous function and $\xi \in [-L, 0]$. It can be further approximated as $R(-L) \sim e^{-2ikL} \frac{1}{-2ik}[e^{2ikL} - 1]$. Therefore, the ratio $R(-L)$ between the impedance gradient and uniform media can be obtained as

$$\left| \frac{R(-L) \quad \text{(gradient)}}{R(-L) \quad \text{(uniform)}} \right| \sim \frac{1}{k} \quad (13)$$

When $\lambda \to 0$ or $k \to \infty$, $L/\lambda = kL/2\pi \to \infty$ led to $\left| \frac{R(-L) \quad \text{(nonuniform)}}{R(-L) \quad \text{(uniform)}} \right| \to 0$. In comparison with uniform material, the impedance gradient material of BMIT significantly suppresses the reflection and then $T \to 1$. Thus, the independent length-wavelength relationship could be demonstrated. The approximate solution at low frequencies ($L/\lambda < 0.25$) might be incorrect because of negative T (Fig. 2). This small reflection approximate theory was based on the assumption of $R << 1$.

For the small impedance perturbation approximation $\gamma(x) = \gamma_0 + \varepsilon' e^{ax}$ (ε' is the perturbation coefficient), we assumed $R = R^{(0)} + \varepsilon' R^{(1)}$ and then derived Eq. 3 into the following leading order and perturbation equations

$$\frac{\partial R^{(0)}(x)}{\partial x} - 2ikR^{(0)}(x) = 0 \quad (14)$$

$$\frac{\partial R^{(1)}(x)}{\partial x} - 2ikR^{(1)}(x) + \frac{ae^{ax}}{2(\gamma_0 + \varepsilon' e^{ax})}[1 - R^{(0)2}(x)] = 0 \quad (15)$$

The reflection coefficients at $x = -L$ of these two equations were further solved as

$$R^{(0)}(-L) = R_0 e^{-2ikL} \quad (16)$$

$$R^{(1)}(-L) = \frac{a}{2} e^{-2ikL} \int_0^{-L} \frac{e^{(a-2ik)x}[1 - R_0^2 e^{4ikx}]}{(\gamma_0 + \varepsilon' e^{ax})} dx \quad (17)$$

Note that this approximate theory required that the impedance perturbation coefficient ε' should be sufficiently smaller than 1, and thus, $\varepsilon' = 0.2$ was used in Fig. 2A. In addition, to investigate the effect of Q on the transmission performance of QIT and BMIT, we calculated their transmission coefficients where $Q = 11.4$ and 32.1 correspond to aluminum and steel, respectively, as shown in Fig. 2B. We also tested the transmission performances of copper ($Q = 28.3$), gold ($Q = 42$), and quartz ($Q = 10.1$), respectively, in fig. S4.

Hydrogel-based design of BMIT

Agarose hydrogels in 3% concentrations with a 60-mm sample thickness were built. Ultrapure agarose powder was measured as 6.48 g by the electronic balance and added to the 216-ml volume of deionized water in a beaker for complete mixing. To avoid water loss during heating, the mixture was covered by a filtering paper. The mixture in the beaker was heated 2 min to boil in a microwave oven. The heated liquid agarose solution was placed in a fabricated cooling tank and cooled down to about 60°C. A hexagonal array of steel cylinders was prepared in an acrylic mold with a dimension of 6 cm by 6 cm by 6 cm. The solution was put into the acrylic mold to compose the steel-hydrogel composite and was slightly overfilled to avoid the formation of bubbles. After solidified, gels were carefully removed from the mold and used for acoustic transmission experiments. Using the method in fig. S2, density, sound speed, and acoustic impedance of agarose hydrogel were measured as 1.017×10^3 kg/m^3, 1517 m/s, and 1.54×10^6 Pa·s/m (fig. S5). For comparison, density, sound speed, and acoustic impedance of steel sample were measured as 7.856×10^3 kg/m^3, 5419 m/s, and 42.57×10^6 Pa·s/m, which are consistent with the literature values [3] and thus verified our experimental procedures.

Determination of the acoustic impedance function of BMIT using metagel

The hexagonal array of steel cylinders with variant radii r was embedded in the agarose hydrogel to achieve the impedance function in Fig. 1B, where the hexagonal lattice constant is $a = 2$ mm and the filling ratio Φ of the steel cylinder satisfies $\Phi = \frac{2\pi r^2}{\sqrt{3}a^2}$. In experiments, the lattice constant of the cylinders was much smaller than the wavelength. The physical effect of effective density and sound speed of BMIT could be understood from the point of view of the effective medium theory (*3*, *30*, *32*). On the basis of the long-wavelength approximation, the effective parameters of the hydrogel-steel composite were described as

$$\rho^* = \Phi\rho_1 + (1 - \Phi)\rho_0,\ c_L^* = \sqrt{\frac{\lambda^* + 2G^*}{\rho^*}},\ \text{and}\ \ c_T^* = \sqrt{\frac{G^*}{\rho^*}} \quad (18)$$

where ρ^*, c_L^*, and c_T^* represent the effective density and sound speeds of longitudinal and transverse waves, respectively. The effective Lamé coefficient and shear modulus satisfy $\lambda^* = \frac{(M-1)G^* + (M+1)G_0 + \lambda_0}{1 - M}$ and $G^* = \frac{G_1(1+\Phi) + G_0(1-\Phi)}{G_1(1-\Phi) + G_0(1+\Phi)} G_0$, respectively, where $M = \frac{[\lambda_1 + G_1 - (\lambda_0 + G_0)]\Phi}{\lambda_1 + G_1 + G_0}$. According to previous studies (*29*–*32*), the densities of hydrogel and steel were used as $\rho_0 = 1070$ kg/m^3 and $\rho_1 = 7800$ kg/m^3, respectively. The Lamé coefficient of hydrogel and steel were used as $\lambda_0 = 2.3$GPa and $\lambda_1 = 107.4$ GPa, respectively. The shear modulus of hydrogel and steel were used as $G_0 = 0.24$ MPa and $G_1 = 84.4$ GPa, respectively. Figure S6 (A to D) shows the effects of the filling ratio Φ on the effective density, the effective sound speed of the longitudinal wave, the effective sound speed of the transverse wave, and the effective longitudinal impedance, respectively, where the parameters of the steel and agarose hydrogel were given for comparisons. With the increase of Φ, the effective density increased from 1070 to 7800 kg/m^3. On the basis of $\Phi = \frac{2\pi r^2}{\sqrt{3}a^2}$, the effect of cylinder diameter on the acoustic impedance could be obtained. Therefore, the acoustic impedance profile in BMIT in Fig. 3B could be obtained.

Fabrication and acoustic transmission experiments of BMIT

We assembled BMIT using agarose hydrogel to embed a hexagonal matrix of steel cylinders. The agarose hydrogel layer (fig. S7) was sandwiched between two acrylic rectangular plates with a dimension of 6 cm by 6 cm by 0.5 cm. The plates were fabricated on the

basis of a hexagonal honeycomb metamaterial design. The hexagonal lattice constant was 2 mm, and the steel cylinder diameter D of BMIT was progressively increased from 0.1 to 2 mm.

To tune the acoustic impedance, the steel-hydrogel composite without two acrylic plates was compressed by pushing the plastic plate at $x = 0$, and the movement was measured with a vernier caliper. Forty percent compression of the steel-hydrogel composite was performed by pushing the plastic plate from $x = 0$ to $x = -0.4L$ using an external force. Using the experimental method in Fig. 2, the acoustic impedance profile in Fig. 1B could be approached for BMIT, and they show a significant linear correlation ($P < 0.001$, $r^2 = 0.98$).

Ultrasound transmission experiments were performed in an anechoic water tank. A tank with dimension of 1.2 m by 1.2 m by 1 m was covered by sound-absorbing material to approach the condition of the free acoustic field. A broadband acoustic transducer with a diameter of 0.03 m was used to produce the tone-burst signal with a five-cycle duration, where the applied frequency range was from 50 to 230 kHz. The signals were recorded by a broadband receiver at a distance of 0.1 m. The signal was then analog to digital (A/D) converted with the sampling rate of 1M kHz. The signals were measured 10 times to test the reproducibility. When the transducer frequency was increased from 60 to 120 kHz and the transformer length was decreased from 2.5 to 1.5 cm, both frequency and length dependencies for maximal transmission are found in QIT; however, BMIT was not influenced by increasing frequency and compression. Frequency shift between theoretical predictions and experimental measurements in Fig. 3C may be associated with the thin water layer between the acoustic transducer and the transformer.

Underwater ultrasound transmission experiments were performed using a single-beam echosounder (BioSonics, Seattle, WA, USA) with a transducer diameter of 26 cm and center frequency of 123 kHz. To fit the sizes of the transformers and reduce the effect of wave reflections, extra spaces of the transducer beyond the transformers were covered by sound-absorbing material. An iron cylinder with a length of 10 cm and a diameter of 9 cm was used as an acoustic ranging object. In Fig. 4, the time-distance acoustic backscatter intensity profiles for QIT and BMIT were given for $L = 2.5$ and 1.5 cm, where the horizontal axis is time, the vertical axis is the ranging distance, and the color bar gives the backscattered signal amplitude in decibel. The echo amplitude significantly increased when the steel wall was detected, while the object has a smaller backscattering area. The steel wall was shown in brown, the object was shown in yellow, and the water was shown in green. We tested the ultrasound detection performances of QIT and BMIT by including the following cases: (I) without object, (II) with an immobile object, and (III) with a swaying object. Decreasing the transformer length to $L = 1.5$ cm at the compression ratio of 40% might not significantly affect underwater ultrasound detection.

SUPPLEMENTARY MATERIALS

Supplementary material for this article is available at http://advances.sciencemag.org/cgi/content/full/6/44/eabb3641/DC1

REFERENCES AND NOTES

1. N. Fang, D. Xi, J. Xu, M. Ambati, W. Srituravanich, C. Sun, X. Zhang, Ultrasonic metamaterials with negative modulus. *Nat. Mater.* **5**, 452–456 (2006).
2. A. N. Norris, Acoustic metafluids. *J. Acoust. Soc. Am.* **125**, 839 (2009).
3. D. Torrent, J. Sánchez-Dehesa, Acoustic metamaterials for new two-dimensional sonic devices. *New J. Phys.* **9**, 323 (2007).
4. K. Melde, A. G. Mark, T. Qiu, P. Fischer, Holograms for acoustics. *Nature* **537**, 518–522 (2016).
5. S. Zhang, C. Xia, N. Fang, Broadband acoustic cloak for ultrasound waves. *Phys. Rev. Lett.* **106**, 024301 (2011).
6. T. Brunet, A. Merlin, B. Mascaro, K. Zimny, J. Leng, O. Poncelet, C. Aristégui, O. Mondain-Monval, Soft 3D acoustic metamaterial with negative index. *Nat. Mater.* **14**, 384–388 (2015).
7. J.-Y. Sun, X. Zhao, W. R. K. Illeperuma, O. Chaudhuri, K. H. Oh, D. J. Mooney, J. J. Vlassak, Z. Suo, Highly stretchable and tough hydrogels. *Nature* **489**, 133–136 (2012).
8. H. Yuk, S. Lin, C. Ma, M. Takaffoli, N. X. Fang, X. Zhao, Hydraulic hydrogel actuators and robots optically and sonically camouflaged in water. *Nat. Commun.* **8**, 14230 (2017).
9. K. Zhang, C. Ma, Q. He, S. Lin, Y. Chen, Y. Zhang, N. X. Fang, X. Zhao, Metagel with broadband tunable acoustic properties over air-water-solid ranges. *Adv. Funct. Mater.* **29**, 1903699 (2019).
10. Y. Gao, J. Song, S. Li, C. Elowsky, Y. Zhou, S. Ducharme, Y. M. Chen, Q. Zhou, L. Tan, Hydrogel microphones for stealthy underwater listening. *Nat. Commun.* **7**, 12316 (2016).
11. J. P. Maxfield, H. C. Harrison, Methods of high quality recording and reproducing of music and speech based on telephone research. *Bell Syst. Tech. J.* **5**, 493–523 (1926).
12. D. M. Pozar, *Microwave Engineering Reading* (Addison-Wesley, MA, 1990), pp. 106–116.
13. L. R. Walker, N. Wax, Non-uniform transmission lines and reflection coefficients. *J. Appl. Phys.* **17**, 1043–1045 (1946).
14. C. Shen, J. Xu, N. X. Fang, Y. Jing, Anisotropic complementary acoustic metamaterial for canceling out aberrating layers. *Phys. Rev. X* **4**, 041033 (2014).
15. M. Dubois, C. Shi, X. Zhu, Y. Wang, X. Zhang, Observation of acoustic Dirac-like cone and double zero refractive index. *Nat. Commun.* **8**, 14871 (2017).
16. Y. Shen, D. Ye, I. Celanovic, S. G. Johnson, J. D. Joannopoulos, M. Soljačić, Optical broadband angular selectivity. *Science* **343**, 1499–1501 (2014).
17. M. S. Eggleston, K. Messer, L. Zhang, E. Yablonovitch, M. C. Wu, Optical antenna enhanced spontaneous emission. *Proc. Natl. Acad. Sci. U.S.A.* **112**, 1704–1709 (2015).
18. K. Pendergraft, R. Pieper, An exact solution for a reflection coefficient in a medium having an exponential impedance profile. *J. Acoust. Soc. Am.* **94**, 580–582 (1993).
19. P. A. Martin, On Webster's horn equation and some generalizations. *J. Acoust. Soc. Am.* **116**, 1381 (2004).
20. Z. Li, D.-Q. Yang, S.-L. Liu, S.-Y. Yu, M.-H. Lu, J. Zhu, S.-T. Zhang, M.-W. Zhu, X.-S. Guo, H.-D. Wu, X.-L. Wang, Y.-F. Chen, Broadband gradient impedance matching using an acoustic metamaterial for ultrasonic transducers. *Sci. Rep.* **7**, 42863 (2017).
21. J. F. Allard, N. Atalla, *Propagation of Sound in Porous Media: Modelling Sound Absorbing Materials* (John Wiley & Sons, Ltd, ed. 2, 2009).
22. W. W. L. Au, K. J. Benoit-Bird, Automatic gain control in the echolocation system of dolphins. *Nature* **423**, 861–863 (2003).
23. W. W. L. Au, *The Sonar of Dolphins* (Springer-Verlag, New York, 1993), 277 p.
24. Z. Song, Y. Zhang, P. Berggren, C. Wei, Reconstruction of the forehead acoustic properties in an Indo-Pacific humpback dolphin (*Sousa chinensis*), with investigation on the responses of soft tissue sound velocity to temperature. *J. Acoust. Soc. Am.* **141**, 681–689 (2017).
25. T. W. Cranford, M. F. Mckenna, M. S. Soldevilla, S. M. Wiggins, J. A. Goldbogen, R. E. Shadwick, P. Krysl, J. A. St. Leger, J. A. Hildebrand, Anatomic geometry of sound transmission and reception in Cuvier's beaked whale (*Ziphius cavirostris*). *Anat. Rec.* **291**, 353–378 (2008).
26. L. N. Kloepper, P. E. Nachtigall, M. J. Donahue, M. Breese, Active echolocation beam focusing in the false killer whale, *Pseudorca crassidens*. *J. Exp. Biol.* **215**, 1306–1312 (2012).
27. D. M. Wisniewska, J. M. Ratcliffe, K. Beedholm, C. B. Christensen, M. Johnson, J. C. Koblitz, M. Wahlberg, P. T. Madsen, Range-dependent flexibility in the acoustic field of view of echolocating porpoises (*Phocoena phocoena*). *eLife* **4**, e05651 (2015).
28. Y. Zhang, Z. Song, X. Wang, W. Cao, W. W. L. Au, Directional acoustic wave manipulation by a porpoise via multiphase forehead structure. *Phys. Rev. Appl.* **8**, 064002 (2017).
29. E. Dong, Y. Zhang, Z. Song, T. Zhang, C. Cai, N. X. Fang, Physical modeling and validation of porpoises' directional emission via hybrid metamaterials. *Natl. Sci. Rev.* **6**, 921–928 (2019).
30. Y. Zhang, X. Gao, S. Zhang, W. Cao, L. Tang, D. Wang, Y. Li, A biomimetic projector with high subwavelength directivity based on dolphin biosonar. *Appl. Phys. Lett.* **105**, 123502 (2014).
31. K. L. Tsakmakidis, L. Shen, S. A. Schulz, X. Zheng, J. Upham, X. Deng, H. Altug, A. F. Vakakis, R. W. Boyd, Breaking Lorentz reciprocity to overcome the time-bandwidth limit in physics and engineering. *Science* **356**, 1260–1264 (2017).
32. J. Mei, Z. Liu, W. Wen, P. Sheng, Effective dynamic mass density of composites. *Phys. Rev. B* **76**, 134205 (2007).
33. Q. Gan, Y. J. Ding, F. J. Bartoli, "Rainbow" trapping and releasing at telecommunication wavelengths. *Phys. Rev. Lett.* **102**, 056801 (2009).
34. H. Ge, M. Yang, C. Ma, M. Lu, Y.-F. Chen, N. Fang, Breaking the barriers: Advances in acoustic functional materials. *Natl. Sci. Rev.* **5**, 159–182 (2017).
35. C. Keplinger, J.-Y. Sun, C. C. Foo, P. Rothemund, G. M. Whitesides, Z. Suo, Stretchable, transparent, ionic conductors. *Science* **341**, 984–987 (2013).

36. S. Lin, X. Liu, J. Liu, H. Yuk, H.-C. Loh, G. A. Parada, C. Settens, J. Song, A. Masic, G. H. McKinley, X. Zhao, Anti-fatigue-fracture hydrogels. *Sci. Adv.* **5**, eaau8528 (2019).
37. J. Wu, G. Du, Analogy between the one-dimensional acoustic waveguide and the electrical transmission line for cases with loss. *J. Acoust. Soc. Am.* **100**, 3973–3975 (1996).

Acknowledgments: We thank P. Cao and L. Tang for their experimental assistance. **Funding:** Y.Z., E.D., S.G.M., Z.S., and Q.H. acknowledge financial support from the National Key Research and Development Program of China (2018YFC1407504) and the National Natural Science Foundation of China (grant nos. 41676023, 41276040, 41422604, and 11604128). **Author contributions:** Y.Z., N.X.F., and X.Z. conceived the project. Y.Z., S.G.M., and Q.H. conducted the analysis of theoretical and numerical data. E.D. and Z.S. provided the numerical simulation and experimental data. E.D. and Z.S. collected and conducted the analyses of experimental data and wrote the manuscript. **Competing interests:** The authors declare that they have no competing interests. **Data and materials availability:** All data needed to evaluate the conclusions in the paper are present in the paper and/or the Supplementary Materials. Additional data related to this paper may be requested from the authors.

Submitted 19 February 2020
Accepted 16 September 2020
Published 30 October 2020
10.1126/sciadv.abb3641

Citation: E. Dong, Z. Song, Y. Zhang, S. Ghaffari Mosanenzadeh, Q. He, X. Zhao, N. X. Fang, Bioinspired metagel with broadband tunable impedance matching. *Sci. Adv.* **6**, eabb3641 (2020).

ScienceAdvances

Bioinspired metagel with broadband tunable impedance matching

Erqian DongZhongchang SongYu ZhangShahrzad Ghaffari MosanenzadehQi HeXuanhe ZhaoNicholas X. Fang

Sci. Adv., 6 (44), eabb3641. • DOI: 10.1126/sciadv.abb3641

Science Advances (ISSN 2375-2548) is published by the American Association for the Advancement of Science. 1200 New York Avenue NW, Washington, DC 20005. The title *Science Advances* is a registered trademark of AAAS.